Chinese Chemical Letters 31 (2020) 1927–1930

Contents lists available at ScienceDirect

Chinese Chemical Letters

journal homepage: www.elsevier.com/locate/cclet

Communication

Solar cells sensitized by porphyrin dyes containing a substituted carbazole donor with synergistically extended absorption and suppressed the dye aggregation

Yunyu Tang[a], Xiujun Liu[b], Yueqiang Wang[b], Qingyun Liu[c,*], Xin Li[d], Chengjie Li[b], Xiaosheng Shen[a,*], Yongshu Xie[b,*]

[a] Laboratory of Quality Safety and Processing for Aquatic Product, East China Sea Fisheries Research Institute, Chinese Academy of Fishery Sciences, Shanghai 200090, China
[b] Key Laboratory for Advanced Materials and Institute of Fine Chemicals, School of Chemistry and Molecular Engineering, East China University of Science and Technology, Shanghai 200237, China
[c] College of Chemical and Environmental Engineering, Shandong University of Science and Technology, Qingdao 266590, China
[d] Division of Theoretical Chemistry and Biology, School of Biotechnology, KTH Royal Institute of Technology, Stockholm SE-10691, Sweden

ARTICLE INFO

Article history:
Received 25 October 2019
Received in revised form 23 December 2019
Accepted 30 December 2019
Available online 31 December 2019

Keywords:
Dye-sensitized solar cells
Porphyrin
Sensitizers
Carbazole
Bulky groups

ABSTRACT

To achieve high power conversion efficiency (*PCE*), three porphyrin sensitizers have been synthesized and explored to simultaneously enhance the photocurrent (J_{sc}) and photovoltage (V_{oc}). On basis of the **XW4**, a benzothiadiazole (BTD) unit has been introduced to afford **XW57** with the aim to extend the absorption wavelength and enhance the light harvesting ability. As a result, a J_{sc} of 13.72 mA/cm^2 has been obtained for **XW57**, higher than that of **XW4**. On this basis, **XW58** has been prepared by modifying the carbazole-based donor with two bulky dihexyloxyphenyl groups, and the superior anti-aggregation character raises the V_{oc} from 781 mV (**XW4**) to 844 mV. When both the BTD unit and the bulky groups are introduced to the acceptor and donor units, respectively, the resulting sensitizer **XW59** exhibits a highest *PCE* value of 7.34% with synergistically enhanced J_{sc} of 13.19 mA/cm^2 and V_{oc} of 793 mV. These results provide further insight into developing high performance dye-sensitized solar cells

With the exhaustion of fossil resources and the related serious environmental pollution problems, it is highly demanded to exploit renewable energy sources. Since 1991, dye-sensitized solar cells (DSSCs) have been developed very fast owing to their relatively high energy-conversion efficiency (*PCE*) and low cost availability [1–3]. To date, lots of excellent dyes have been successfully developed, which can be classified as ruthenium complex sensitizers [4], metal-free organic dyes [5–7] and porphyrin dyes [8,9]. Among them, porphyrins are particularly promising due to their structural similarity to chlorophylls, strong absorption, excellent redox behavior and high efficiencies [10–21]. However, despite the strong light absorption in the Soret (400–450 nm) and Q (550–650) bands, obvious absorption drawbacks of porphyrins are observed in the near-infrared (NIR) region, which limits the light-harvesting in this range [22–25]. To address this issue, rational design of porphyrin dyes has been demonstrated to be effective. For example, the insertion of a triple bond between the donor group and the porphyrin framework was applied in a number of dyes [10,18,26]. Recently, incorporating an auxiliary electron accepting benzothiadiazole (BTD) unit has been demonstrated to be an effective approach for extending the π-conjugation and shifting the absorption to longer wavelengths [27–29]. However, one adverse effect of these approaches is the severe dye aggregation and charge recombination induced by the extended π-conjugated framework, which may result in decreased photovoltages (V_{oc}) [30–32]. To overcome this disadvantage, introduction of multiple bulky groups to the donor may be effective for improving the V_{oc} by suppressing the dye aggregation [33–37]. In addition, electrolyte is also an important factor for achieving efficient DSSCs [38]. In this regard, the Co^{3+}/Co^{2+} based electrolyte has been widely used in recent years owing to their weak visible light absorption, high photovoltages induced by its higher redox potential and weak corrosiveness towards metallic conductors [39–41].

* Corresponding authors.
E-mail addresses: qyliu@sdust.edu.cn (Q. Liu), foodsmc98@126.com (X. Shen), yshxie@ecust.edu.cn (Y. Xie).

https://doi.org/10.1016/j.cclet.2019.12.038
1001-8417/

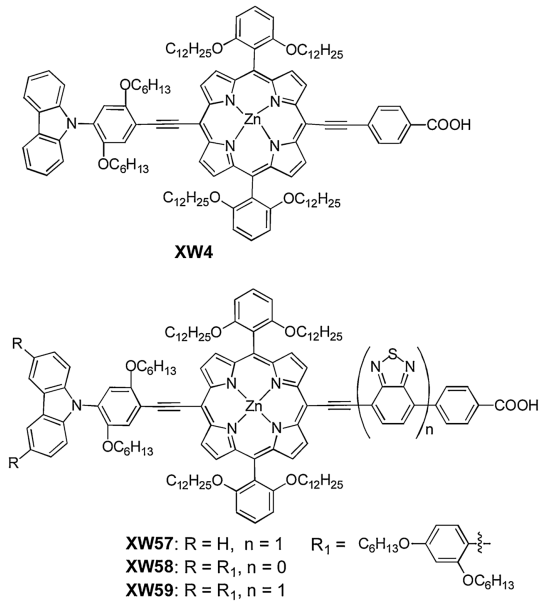

Fig. 1. Molecular structures of porphyrin dyes **XW4** and **XW57-XW59**.

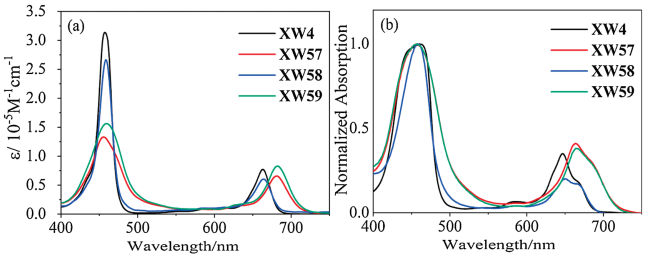

Fig. 2. Absorption spectra of dyes **XW4** and **XW57-XW59**. (a) in THF solutions, (b) on TiO_2 films (3 μm in thickness).

Herein, we report a series of novel porphyrin dyes by modifying **XW4** [8]. Initially, **XW57** (Fig. 1) was designed by incorporating a BTD unit as the auxiliary acceptor to improve the light harvesting ability in the NIR region. As expected, it exhibits a higher photocurrent (J_{sc}) value (13.72 mA/cm^2) than that of **XW4** (12.82 mA/cm^2). On the other hand, the carbazole donor group was further modulated by introducing bulky dihexyloxyphenyl groups to afford **XW58**, which is finally wrapped with ten alkoxy chains. Consequently, it exhibits a relatively higher V_{oc} value of 844 mV relative to those of **XW4** and **XW57**, which mainly result from the efficient suppression of dye aggregation, accompanied with preventing the Co^{3+}/Co^{2+} ions in the electrolyte from approaching the TiO_2 surface. The respective strategy of long wavelength absorption (higher J_{sc}) or anti-aggregation (higher V_{oc}) results in enhanced efficiencies of 7.15% (**XW57**) and 6.54% (**XW58**), compared with that of **XW4** (6.49%) using the cobalt electrolyte. By combining these two approaches, we further designed and synthesized **XW59**. The simultaneous improvement of J_{sc} and V_{oc} has been achieved through red-shifted absorption and suppressed dye aggregation. Finally, the DSSCs based on **XW59** exhibit the highest photovoltaic efficiency of 7.34% using the cobalt electrolyte.

The synthetic routes for the porphyrin dyes **XW57**–**XW59** are depicted in Scheme S1 (Supporting information). The donor and acceptor moieties were successively introduced to the porphyrin framework *via* Sonogashira cross-coupling reactions, and the target products were finally obtained by hydrolysis of the ester to generate the anchoring carboxylic groups. All the synthetic products have been fully characterized by NMR and mass spectra (Figs. S1–S13 in Supporting information).

The UV–vis absorption spectra of **XW4** and **XW57**–**XW59** in THF are shown in Fig. 2a, with the corresponding data listed in Table S1 (Supporting information). **XW58** displays a typical intense Soret band around 459 nm and a less intense Q band around 664 nm. Compared with **XW4**, the bulky dihexyloxyphenyl groups introduced in **XW58** cause negligible red-shift of both Soret and Q bands. Similarly, slightly red-shifted absorption spectrum is observed for **XW59**, compared with that of **XW57**. On the other hand, incorporation of the BTD groups into **XW57** and **XW59** leads to dramatically broadened absorption and red-shifted Q-bands centered around 683 nm with a striking absorption onset at *ca.* 734 nm. This observation can be rationalized by the strengthened intramolecular charge transfer (ICT) effect due to the strong electron-deficient character of the BTD unit. The broadened and red-shifted absorption spectra are favorable for light-harvesting and are expected to afford better cell performance. Upon anchoring to 3 μm thick TiO_2 films, all three dyes exhibit blue-shifted Q bands relative to those in THF (Table S1 and Fig. S14 in Supporting information) because of the combined effect of deprotonation and aggregation [42]. Notably, insertion of the auxiliary BTD unit in **XW57** results in a blue shift of *ca.* 19 nm, more obvious than that of 16 nm observed for **XW4**, denoting aggravated H-type aggregation [15] resulting from BTD unit induced π-conjugation framework extension. A similar trend is also observed between **XW58** and **XW59**.

On the other hand, the corresponding blue-shift of *ca.* 14 nm observed for **XW58** is smaller than that observed for **XW4** (16 nm), indicating that the bulky groups attached on the carbazole donor effectively suppress the aggregation. Similar observations could be found between **XW57** and **XW59**. Finally, the trend of blue shifts on TiO_2 films lie in the order of **XW58** < **XW4** < **XW59** < **XW57**, which is consistent with the sequence of the adsorption amounts, *i.e.*, 3.84×10^{-8}, 4.02×10^{-8}, 4.31×10^{-8} and 4.55×10^{-8} mol/cm^2 for **XW58**, **XW4**, **XW59**, and **XW57**, respectively (Table S4 in Supporting information). On the other hand, both the Soret band and Q-bands are broadened due to interactions between dye molecules and/or between the dyes and nanocrystalline TiO_2, (Fig. 2b and Fig. S14), which is beneficial for further improving light-harvesting ability and enhancing J_{sc}.

Cyclic voltammetry was employed to investigate the oxidation potentials and evaluate the possibility of electron injection and dye regeneration from the thermodynamic point of view (Table S1 and Fig. S15 in Supporting information). The estimated ground-state oxidation potentials (E_{ox}) of **XW57**–**XW59** were found to be 0.88 V, 0.85 V and 0.87 V, respectively (Table S1) *vs.* normal hydrogen electrode (NHE), which are obviously more positive than the potential of the Co^{3+}/Co^{2+} redox couple (~0.56 V), indicative of enough driving forces for regenerating the dyes. In addition, the excited-state oxidation potentials (E_{ox}^*) of **XW57**–**XW59** were calculated to be -0.92 V, -1.00 V and -0.92 V, respectively. All these E_{ox}^* values are more negative than that of the TiO_2 conduction band (~-0.5 V), energetically allowing efficient electron injection into TiO_2 from the excited sensitizers [43].

To further understand the structure dependent electron distribution in the frontier molecular orbitals and the absorption spectra, we employed density functional theory (DFT), and time-dependent density functional theory (TDDFT) calculations using the Gaussian 09 program package [44–47]. The electrons of the HOMOs of **XW57**–**XW59** mainly distribute over the carbazole donor moiety and porphyrin, while the LUMOs predominantly delocalized over the carboxyphenyl acceptor moiety and porphyrin (Fig. S17 in Supporting information). Thus, electron transfer from

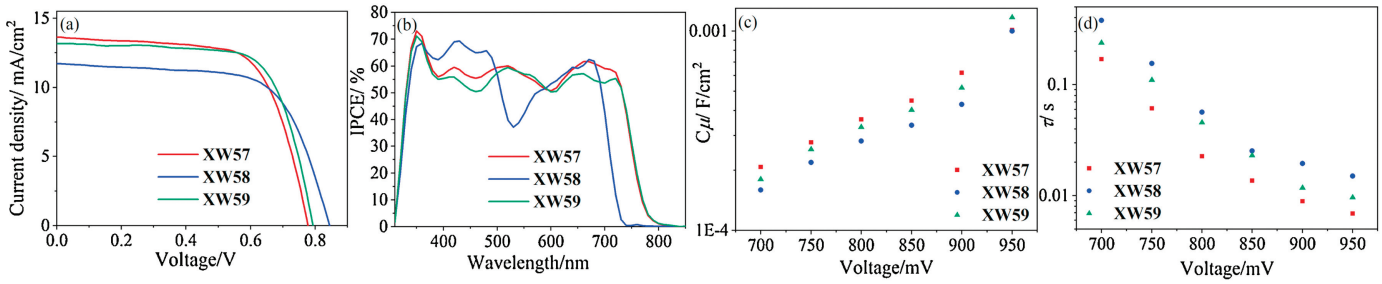

Fig. 3. (a) *J–V* curves, (b) IPCE action spectra, plots of (c) C_μ and (d) τ *versus* potential bias for DSSCs based on **XW57**–**XW59**.

the HOMO to the LUMO can be easily accessible from the donor to the anchoring carboxyphenyl moiety, enabling electron injection from the LUMO to the conduction band of TiO_2. The simulated absorption spectra are shown in Fig. S18 (Supporting information), and the corresponding data are listed in Tables S2 and S3 (Supporting information). The trend of theoretical results for **XW57**–**XW59** is in good agreement with that obtained from the absorption spectra.

The photovoltaic performances of **XW57**–**XW59** were tested using the cobalt-based electrolyte. The corresponding photocurrent density–voltage (*J–V*) curves and monochromatic incident photon to current conversion efficiency (IPCE) spectra are shown in Fig. 3, with the corresponding photovoltaic parameters (J_{sc}, V_{oc}, *FF*, *PCE*) listed in Table 1. The IPCE spectra for all three dyes exhibit a broad spectral response within a large wavelength range (Fig. 3b), indicating that all the dyes can efficiently convert the visible light into photocurrent. Notably, remarkably broadened IPCE action spectra, absorbing in the panchromatic visible region and part of the NIR region, were achieved for **XW57** and **XW59** owing to the presence of the BTD unit in the molecules. Both **XW57** and **XW59** exhibit dramatically red-shifted IPCE onset wavelengths of *ca.* 820 nm relative to that of 740 nm for **XW58**. Introduction of the BTD unit leads to stronger intramolecular charge transfer effect, resulting in the broadened visible region absorption. As a result, J_{sc} values of 13.72 and 13.19 mA/cm^2 were obtained for **XW57** and **XW59**, respectively, in comparison to an obviously lower J_{sc} value of 11.79 mA/cm^2 for **XW58** (Fig. 3a). Compared with **XW4** (12.82 mA/cm^2, 781 mV), **XW57** shows a higher J_{sc} and a lower V_{oc}. These observations may be rationalized by the introduction of the BTD unit which gives the broadened IPCE but more severe dye aggregation. Finally, a higher efficiency of 7.15% was achieved for **XW57**, compared with that of 6.49% obtained for **XW4**. On the other hand, **XW58** exhibits the highest V_{oc} of 844 mV owing to its relatively small π-conjugation size and the presence of the bulky alkoxy chains on the carbazole unit, which is favorable for suppressing the dye aggregation and preventing the Co^{3+}/Co^{2+} ions in the electrolyte from approaching the TiO_2 surface [48–50]. However, a dramatic increase of V_{oc} for **XW58** is accompanied with the sacrifice of J_{sc}.

As a result, **XW58** exhibits an efficiency of 6.54%, slightly higher than that of **XW4** (6.49%), but lower than that of **XW57** in spite of its higher V_{oc}, indicating that synergistic enhancement of V_{oc} and J_{sc} is necessary for achieving good photovoltaic performance. Thus, **XW59** contains both additional alkoxy chains/bulky groups and a BTD unit, which may effectively suppress dye aggregation and charge recombination as well as broadening the absorption. As expected, the J_{sc} and V_{oc} values of **XW59** are simultaneously enhanced to 793 mV and 13.19 mA/cm^2, respectively, afford the highest efficiency of 7.34%. Finally, the *PCEs* follow the order of **XW4** (6.49%) ≈ **XW58** (6.54%) < **XW57** (7.15%) < **XW59** (7.34%).

Table 1
Photovoltaic parameters of the solar cells sensitized by **XW4** and **XW57-XW59** under simulated AM 1.5 G full sunlight (100 mW/cm^2). The active area is 0.12 cm^2.

Dyes	V_{oc} (mV)	J_{sc} (mA/cm^2)	*FF* (%)	*PCE* (%)
XW4	781 ± 4	12.82 ± 0.25	0.65 ± 0.02	6.49 ± 0.12
XW57	778 ± 3	13.72 ± 0.21	0.67 ± 0.02	7.15 ± 0.13
XW58	844 ± 6	11.79 ± 0.11	0.66 ± 0.01	6.54 ± 0.11
XW59	793 ± 2	13.19 ± 0.09	0.70 ± 0.01	7.34 ± 0.16

Generally, alteration of the photovoltage originates from a shift of the TiO_2 electron *quasi*-Fermi-level, which may be related to two main reasons: (i) a shift in the TiO_2 conduction band edge (E_{CB}), which can be evidenced from the chemical capacitance (C_μ), and (ii) fluctuation of electron density, which is related to the electron lifetime (τ) governed by the charge recombination rate [51,52]. Thus, electrochemical impedance spectroscopy (EIS) was recorded in the dark at a series of bias voltages to obtain the corresponding C_μ and τ values. As shown in Fig. 3c, the C_μ values of the cells at a fixed bias voltage rank in the order of **XW58** < **XW59** < **XW57**, indicative of more positive shifts of the TiO_2 conduction band, consistent with the order of the decreasing V_{oc} values. In addition, the electron lifetimes of **XW58** and **XW59**-based cells are longer than those based on **XW57** (Fig. 3d), indicating that **XW57** suffers from more serious dye-aggregation/charge recombination induced by the absence of the bulky groups, which leads to the lowest observed V_{oc} value (*vide supra*). On the other hand, the electron lifetime for **XW58** is longer than that of **XW59**, which may be related to its relatively small conjugation framework. These results indicate that the V_{oc} values of the porphyrin dye-sensitized cells are governed by both the TiO_2 conduction band position and the charge recombination rate.

In summary, three porphyrin dyes **XW57**–**XW59** have been rationally designed and synthesized by introducing bulky substituents into the carbazole-based donor as well as an auxiliary electron-accepting BTD group. As expected, introduction of a strong electron accepting BTD unit in **XW57** resulted in a remarkably red-shifted and broadened Soret band in the range of 400–500 nm. While the onset wavelength of absorption was red-shifted from 695 nm (**XW4**) to 730 nm due to the larger π-conjugation framework and the stronger intramolecular charge transfer complex induced by the BTD unit, which will be favorable for harvesting sunlight in the NIR region. Thus, the IPCE of **XW57** shows extremely red-shifted onset wavelength of *ca.* 820 nm, resulting in a higher J_{sc} value of 13.72 mA/cm^2 than that of 12.82 mA/cm^2 for **XW4**. However, the V_{oc} value of **XW57** was undesirably decreased due to the more severe dye aggregation caused by the larger conjugation framework. As a result of the contradictory effects on J_{sc} and V_{oc}, **XW57** exhibits an efficiency of 7.15%, higher than that of 6.49% obtained for **XW4**. On the other hand, **XW58** exhibits the highest V_{oc} value of 844 mV, which may be ascribed to the least aggregation owing to both the absence of the BTD unit and the presence of additional bulky groups attached at the carbazole unit against π-π interaction and approaching

of Co^{3+}/Co^{2+} in the electrolyte to the TiO_2 surface. At last, accompanied with a sacrifice of J_{sc}, **XW58** exhibits an efficiency of 6.54%. In the sensitizer **XW59**, a BTD unit and the alkoxy chains/bulky groups were simultaneously introduced, and thus the highest *PCE* value of 7.34% was achieved, with simultaneously enhanced J_{sc} (13.19 mA) and V_{oc} (793 mV), when compared to those of **XW4**. It is noteworthy that the rational modulation of the carbazole-based donor by introducing the bulky groups together with the introduction of a benzothiadiazole unit as an extra auxiliary electron acceptor can simultaneously broaden the absorption and suppress the dye aggregation/charge recombination. These results may provide new strategy to develop efficient DSSCs by synergistically enhanced photovoltage and photocurrent.

Declaration of competing interest

The authors declare that they have no known competing financial interests or personal relationships that could have appeared to influence the work reported in this paper.

Acknowledgments

This work was financially supported by Central Public-interest Scientific Institution Basal Research Fund, ECSFR, CAFS (No. 2018T02), the National Natural Science Foundation of China (Nos. 21772041, 21811530005, 21971063, U1707602), and the Fundamental Research Funds for the Central Universities (Nos. WK1616004, 222201717003).

Appendix A. Supplementary data

Supplementary material related to this article can be found, in the online version, at doi:https://doi.org/10.1016/j.cclet.2019.12.038.

References

[1] B. O'Regan, M. Grätzel, Nature 353 (1991) 737–740.
[2] H. Tian, S.C. Huang, S.C. Zhou, Acta Phys. Chim. Sin. 4 (1988) 314–319.
[3] A. Yella, H.W. Lee, H.N. Tsao, et al., Science 334 (2011) 629–634.
[4] M.K. Nazeeruddin, A. Kay, I. Rodicio, et al., J. Am. Chem. Soc. 115 (1993) 6382–6390.
[5] Y.J. Xie, Z. Li, Mater. Chem. Front. 4 (2020) 317–331.
[6] T. Hua, Z.S. Huang, K. Cai, et al., Electrochim. Acta 302 (2019) 225–233.
[7] B. Pan, Y.Z. Zhu, D. Ye, et al., New J. Chem. 42 (2018) 4133–4141.
[8] Y. Wang, B. Chen, W. Wu, et al., Angew. Chem. Int. Ed. 53 (2014) 10779–10783.
[9] Y. Xie, Y. Tang, W. Wu, et al., J. Am. Chem. Soc. 137 (2015) 14055–14058.
[10] Y. Tang, Y. Wang, X. Li, et al., ACS Appl. Mater. Interfaces 7 (2015) 27976–27985.
[11] K. Zeng, Y. Lu, W. Tang, et al., Chem. Sci. 10 (2019) 2186–2192.
[12] Y. Lu, H. Song, X. Li, et al., ACS Appl. Mater. Interfaces 11 (2019) 5046–5054.
[13] Y. Xie, W. Wu, H. Zhu, et al., Chem. Sci. 7 (2016) 544–549.
[14] Y. Lu, Y. Cheng, C. Li, et al., Sci. China Chem. 62 (2019) 994–1000.
[15] H. Song, Q. Liu, Y. Xie, Chem. Commun. 54 (2018) 1811–1824.
[16] M. Urbani, M. Grätzel, M.K. Nazeeruddin, Chem. Rev. 114 (2014) 12330–12396.
[17] Y.Q. Wang, L. Xu, X.D. Wei, et al., New J. Chem. 38 (2014) 3227–3235.
[18] Y. Lu, Q. Liu, J. Luo, et al., ChemSusChem 12 (2019) 2802–2809.
[19] K.W. Zeng, W.Q. Tang, C.J. Li, et al., J. Mater. Chem. A 7 (2019) 20854–20860.
[20] C.J. Li, J.L. Zhang, J.X. Song, et al., Sci. China Chem. 61 (2018) 511–514.
[21] H.L. Song, J. Zhang, J.M. Jin, J. Mater. Chem. C 6 (2018) 3927–3936.
[22] A. Yella, C.L. Mai, S.M. Zakeeruddin, et al., Angew. Chem. Int. Ed. 53 (2014) 2973–2977.
[23] Y.C. Chang, C.L. Wang, T.Y. Pan, Chem. Commun. 47 (2011) 8910–8912.
[24] M.K. Nazeeruddin, F. De Angelis, S. Fantacci, et al., J. Am. Chem. Soc. 127 (2005) 16835–16847.
[25] C.H. Wu, M.C. Chen, P.C. Su, et al., J. Mater. Chem. A 2 (2014) 991–999.
[26] V. Piradi, X. Xu, Z. Wang, et al., ACS Appl. Mater. Interfaces 11 (2019) 6283–6291.
[27] Z. Yao, H. Wu, Y. Ren, et al., Energy Environ. Sci. 8 (2015) 1438–1442.
[28] P. Gautam, R. Misra, S.A. Siddiqui, et al., ACS Appl. Mater. Interfaces 719 (2015) 10283–10292.
[29] H. Zhu, W. Li, Y. Wu, et al., ACS Sustain. Chem. Eng. 2 (2014) 1026–1034.
[30] J.P. Hill, Angew. Chem. Int. Ed. 55 (2016) 2976–2978.
[31] H.P. Wu, Z.W. Ou, T.Y. Pan, et al., Energy Environ. Sci. 5 (2012) 9843–9848.
[32] M. Zhang, Y. Wang, M. Xu, et al., Energy Environ. Sci. 6 (2013) 2944–2949.
[33] H.L. Jia, M.D. Zhang, W. Yan, et al., J. Mater. Chem. A 4 (2016) 11782–11788.
[34] W.I. Hung, Y.Y. Liao, T.H. Lee, et al., Chem. Commun. 51 (2015) 2152–2155.
[35] X. Zhang, J. Mao, D. Wang, et al., ACS Appl. Mater. Interfaces 7 (2015) 2760–2771.
[36] Z. Wang, M. Liang, Y. Tan, et al., J. Mater. Chem. A 3 (2015) 4865–4874.
[37] X. Li, Z. Zheng, W. Jiang, et al., Chem. Commun. 51 (2015) 3590–3592.
[38] S.A. Sapp, C.M. Elliott, C. Contado, et al., J. Am. Chem. Soc. 124 (2002) 11215–11222.
[39] Y. Hao, Y. Saygili, J. Cong, et al., ACS Appl. Mater. Interfaces 8 (2016) 32797–32804.
[40] H.N. Tsao, T. Moehl, J.H. Yum, et al., ChemSusChem 4 (2011) 591–594.
[41] S.M. Feldt, E.A. Gibson, E. Gabrielsson, et al., J. Am. Chem. Soc. 132 (2010) 16714–16724.
[42] L. Zhang, J.M. Cole, J. Mater. Chem. A 5 (2017) 19541–19559.
[43] H.H. Chou, K.S.K. Reddy, H.P. Wu, et al., ACS Appl. Mater. Interfaces 8 (2016) 3418–3427.
[44] M.J. Frisch, G.W. Trucks, H.B. Schlegel, et al., Gaussian 09 Revision A.2, Gaussian Inc., Wallingford CT, 2009.
[45] A.D. Becke, J. Chem. Phys. 98 (1993) 5648–5652.
[46] C. Lee, W. Yang, R.G. Parr, Phys. Rev. B 37 (1988) 785–789.
[47] W.J. Hehre, R. Ditchfield, J.A. Pople, J. Chem. Phys. 56 (1972) 2257–2261.
[48] P. Dai, H. Dong, M. Liang, et al., ACS Sustain. Chem. Eng. 5 (2017) 97–104.
[49] Y.K. Eom, S.H. Kang, I.T. Choi, et al., J. Mater. Chem. A 5 (2017) 2297–2308.
[50] Y. Ren, D. Sun, Y. Cao, et al., J. Am. Chem. Soc. 140 (2018) 2405–2408.
[51] T. Wei, X. Sun, X. Li, et al., ACS Appl. Mater. Interfaces 7 (2015) 21956–21965.
[52] G. Yang, Y. Tang, X. Li, et al., ACS Appl. Mater. Interfaces 9 (2017) 36875–36885.